PDGF may be a physiological inducer of Lerk2 phosphorylation, because many types of central nervous system neurons express PDGF β receptors and respond to PDGF, including neurons of the cerebral cortex, which are known to express Lerk2 (*13*, *30*).

The suppression of mitogenic signaling by Lerk2 may be part of a negative feedback loop, which would reduce the cell's responsiveness to peptide growth factors. Possible mechanisms of action may involve the recruitment of cytoplasmic phosphotyrosine phosphatases (*31*), which could antagonize signaling pathways downstream of RTKs, or of cytoplasmic tyrosine kinases such as Abl, which mediates growth inhibitory effects by interacting with the cell cycle machinery (*32*) and is implicated in axonal pathfinding (*33*). Whatever the mechanism, the discovery of regulated tyrosine phosphorylation of ligands for Eph receptors will rapidly advance our understanding of axonal guidance and possibly of cell growth in the developing embryo.

REFERENCES AND NOTES

1. S. Davis *et al.*, *Science* **266**, 816 (1994).
2. R. Brambilla *et al.*, *EMBO J.* **14**, 3116 (1995).
3. R. Brambilla and R. Klein, *Mol. Cell. Neurosci.* **6**, 487 (1995).
4. N. W. Gale *et al.*, *Neuron* **17**, 9 (1996).
5. U. Drescher *et al.*, *Cell* **82**, 359 (1995).
6. H.-J. Cheng, M. Nakamoto, A. D. Bergemann, J. G. Flanagan, *ibid.*, p. 371.
7. Q. Xu, G. Alldus, R. Macdonald, D. G. Wilkinson, N. Holder, *Nature* **381**, 319 (1996).
8. M. Nakamoto *et al.*, *Cell* **86**, 755 (1996).
9. M. Henkemeyer *et al.*, *Oncogene* **9**, 1001 (1994).
10. E. B. Pasquale, *Cell Regul.* **2**, 523 (1991).
11. N. Becker *et al.*, *Mech. Dev.* **47**, 3 (1994).
12. M. Henkemeyer *et al.*, *Cell* **86**, 35 (1996).
13. D. Orioli, M. Henkemeyer, G. Lemke, R. Klein, T. Pawson, *EMBO J.* **15**, 6035 (1996).
14. J. A. Holash and E. B. Pasquale, *Dev. Biol.* **172**, 683 (1995).
15. M. P. Beckmann *et al.*, *EMBO J.* **13**, 3757 (1994).
16. B. D. Bennett *et al.*, *Proc. Natl. Acad. Sci. U.S.A.* **92**, 1866 (1995).
17. A. D. Bergemann, H.-J. Cheng, R. Brambilla, R. Klein, J. G. Flanagan, *Mol. Cell. Biol.* **15**, 4921 (1995).
18. N. A. Nicola *et al.*, *Growth Factors* **13**, 141 (1996).
19. N. W. Gale *et al.*, *Oncogene* **13**, 1343 (1996).
20. Z. Songyang and L. C. Cantley, *Trends Biochem. Sci.* **20**, 470 (1995).
21. N. Stahl *et al.*, *Science* **267**, 1349 (1995).
22. P. Bork and B. Margolis, *Cell* **80**, 693 (1995).
23. T. Pawson, *Nature* **373**, 573 (1995).
24. Generation and culture of NIH 3T3–derived cell lines were done as described (*2*). For immunoprecipitation analysis, cells were washed twice with phosphate-buffered saline and lysed in Triton-LB [50 mM tris (pH 7.5), 1% Triton X-100, 50 mM NaCl, and 50 mM NaF] with protease inhibitors (Complete, Boehringer), pepstatin, and 0.1 mM sodium orthovanadate. For tissue lysis, 0.5 mM sodium orthovanadate, 10 mM disodium b-glycerophosphate, and 20 mM disodium p-nitrophenylphosphate (Sigma) were additionally included. Polyclonal antiserum to Lerk2A (anti-Lerk2A) was raised against the following COOH-terminal Lerk2 peptide: NH_2-HYEKVSGDYGHPVY-COOH (*34*). Polyclonal anti-Lerk2B was raised against a GST-Lerk2 cytoplasmic domain fusion protein (GST-Lerk2 cyto.) expressed in bacteria and purified by glutathione Sepharose (Pharmacia) affinity chromatography. Additional polyclonal antisera included anti-HAp against the hemagglutinin tag (HA.11, Babco), anti–PDGF receptor (anti-PDGFR), and anti-cst1 against Src family kinases (from S. Courtneidge and G. Alonso). Mouse monoclonal antibodies included anti-HAm against the hemagglutinin tag (12CA5, Boehringer); anti-PY against phosphotyrosine (4G10, UBI); and 2-17, specific for Src (from S. Courtneidge and P. Lock).
25. Cek5-Fc and Lerk2-Fc fusion proteins (from Y. Whang-Zhu) were expressed and affinity-purified by Affigel protein A columns as described [H. Shao *et al.*, *J. Biol. Chem.* **269**, 26606 (1994)].
26. K. Brückner, E. B. Pasquale, R. Klein,data not shown.
27. Immunoprecipitates were subjected to kinase assays as described [R. M. Kypta *et al.*, *Cell* **62**, 481 (1990)]. Purified GST fusion proteins or acid-denatured enolase were added as exogenous substrates. The SH3 domain of the Fyn kinase was expressed as GST fusion protein (from P. Lock).
28. E. B. Pasquale, R. J. Connor, D. Rocholl, H. Schnürch, W. Risau, *Dev. Biol.* **163**, 491 (1994).
29. S. Holland *et al.*, *Nature* **383**, 722 (1996).
30. A. Smits *et al.*, *Proc. Natl. Acad. Sci. U.S.A.* **88**, 8159 (1991).
31. R. F. Paulson, S. Vesely, K. A. Siminovitch, A. Bernstein, *Nature Genet.* **13**, 309 (1996).
32. A. Goga *et al.*, *Oncogene* **11**, 791 (1995).
33. F. B. Gertler, R. L. Bennett, M. J. Clark, F. M. Hoffmann, *Cell* **58**, 103 (1989).
34. Single-letter abbreviations for the amino acid residues are as follows: D, Asp; E, Glu; G, Gly; H, His; K, Lys; P, Pro; S, Ser; V, Val; and Y, Tyr.
35. Focus-formation assays on NIH 3T3 cells were done as described [R. Klein *et al.*, *Cell* **66**, 395 (1991)], with the use of the following expression plasmids (the amount of DNA per 10-cm dish is given in brackets): TrkB (pFRK46; 500 ng), BDNF (pLL42; 10 ng), PDGF B-B {pSV7d-PDGF-B1; 5 ng [A. Östmann *et al.*, *J. Biol. Chem.* **268**, 16202 (1988)]}, pMEXneo (500 ng), Lerk2wt (pRB29; 500 ng), Lerk2ΔC (pRB49; 500 ng) (*2*); H-Ras^{Leu61} (pRB34; 50 ng); and Src^{Phe527} {pSGTSrc527; 50 ng [T. Erpel *et al.*, *EMBO J.* **14**, 963 (1995)]}.

36. We thank S. Courtneidge, P. Lock, G. Alonso, C.-H. Heldin, and Y. Wang-Zhu for reagents; R. Brambilla for cell lines; F. Peverali, A. Nebreda, G. Lemke, and T. Graf for helpful discussions; and G. Superti-Furga, P. Orban, and R. Adams for critically reading the manuscript. K.B. is supported by an EMBL predoctoral fellowship. Supported in part by grants from the Deutsche Forschungsgemeinschaft (Kl 948/1-1) and NIH (EY10576).

30 September 1996; accepted 27 January 1997

Spatially and Functionally Distinct Ca^{2+} Stores in Sarcoplasmic and Endoplasmic Reticulum

Vera A. Golovina and Mordecai P. Blaustein*

The organization of calcium (Ca^{2+}) stores in the sarcoplasmic and endoplasmic reticulum (S-ER) is poorly understood. The dynamics of the storage and release of calcium in the S-ER of intact, cultured astrocytes and arterial myocytes were studied with high-resolution imaging methods. The S-ER appeared to be a continuous tubular network; nevertheless, calcium stores in the S-ER were organized into small, spatially distinct compartments that functioned as discrete units. Cyclopiazonic acid (an inhibitor of the calcium pump in the S-ER membrane) and caffeine or ryanodine unloaded different, spatially separate compartments. Heterogeneity of calcium stores was also revealed in cells activated by physiological agonists. These results suggest that cells can generate spatially and temporally distinct calcium signals to control individual calcium-dependent processes.

Activation of most cells evokes diverse and complex responses that depend on mobilization of Ca^{2+} from intracellular stores in the sarcoplasmic (in muscle) or endoplasmic reticulum (S-ER) (*1*). Two types of S-ER Ca^{2+} stores have been functionally characterized (*1–4*) and identified by immunocyto-chemical localization of receptors (*5*). Release of Ca^{2+} from one of the stores requires *myo*-inositol 1,4,5-trisphosphate (IP_3) (*1*). Thapsigargin (TG) (*2–4*, *6*, *7*) and cyclopiazonic acid (CPA) (*3*, *7*, *8*), irreversible and reversible inhibitors of the Ca^{2+} pump in the S-ER membrane, respectively, deplete this IP_3-sensitive store. Mobilization of Ca^{2+} from the IP_3-insensitive store requires cytosolic Ca^{2+} in the micromolar range (*9*) and can be activated by caffeine (CAF) (*10*) and either activated or blocked by ryanodine (RY), depending on the concentration (*11*). In some cells, neither TG nor CPA depletes the CAF- and RY-sensitive Ca^{2+} store, suggesting that there is also a TG- and CPA-resistant S-ER Ca^{2+} pump (*2–4*).

The S-ER appears to be a continuous, interconnected network of tubules (*12*). It remains unclear, however, whether the pharmacologically identified stores are spatially separate (*1–4*) because the two S-ER Ca^{2+} stores have not been directly visualized. To perform dynamic high-resolution imaging studies in intact, primary cultured astrocytes and mesenteric artery (MA) myocytes (*13*), we loaded intracellular organelles preferentially (*14*) with the Ca^{2+}-sensitive, ratiometric fluorochromes furaptra (Figs. 1 and 2), fura-2FF

Department of Physiology and Center for Vascular Biology and Hypertension, University of Maryland School of Medicine, Baltimore, MD 21201, USA.

*To whom correspondence should be addressed.

(*15*), and fura-2 (Fig. 3).

In cells loaded with furaptra (dissociation constant $K_d \approx 54$ μM for Ca^{2+}) at 22°C (*14*), dye distributed throughout the cytoplasm (Fig. 1A); therefore, most of the furaptra leaked out of cells permeabilized with saponin in Ca^{2+}-free medium (Fig. 1, B and C) (*16*, *17*). Initially, most of the furaptra signal came from the cytosol, where the concentration of free Ca^{2+} ($[Ca^{2+}]_{cyt}$) is ≈0.1 μM (*8*, *18*, *19*); only dye within the organelles remained after treatment with saponin, and the calculated $[Ca^{2+}]$ (*20*) rose (Fig. 1C). In contrast, when furaptra was loaded at 36°C (*14*, *21*), as in all subsequent experiments, most of the intracellular dye was sequestered in organelles (Fig. 1D), where it was hydrolyzed to impermeant furaptra; little dye was released by subsequent saponin permeabilization of the plasmalemma (Fig. 1, E and F). Under these conditions, the Ca^{2+} concentration, presumably "free" Ca^{2+} within stores, was initially high (≈100 μM), and saponin induced little change (Fig. 1F). This suggests that the intraorganellar $[Ca^{2+}]$ can be estimated directly in nonpermeabilized cells. Furaptra is, however, also sensitive to Mg^{2+} ($K_d \approx 1.5$ mM) (*22*, *23*); thus, some of the signal may come from Mg^{2+}-furaptra complexes. Therefore, fura-2FF and fura-2, which are Ca^{2+} selective, were used similarly (Fig. 3).

Unloading and reloading of Ca^{2+} in visually identifiable stores of intact (nonpermeabilized) cells was studied at higher magnification (Figs. 2 through 4). Furaptra (Fig. 2A), 3,3′-dihexyloxacarbocyanine (DiOC)–stained (Fig. 2B) (*24*), and Ca^{2+} images (Fig. 2D) were made of a small peripheral portion of a MA myocyte. The Ca^{2+} concentration within the S-ER ($[Ca^{2+}]_{S\text{-}ER}$) was imaged before mobilization of stored Ca^{2+} (Fig. 2D). The S-ER was later stained with the lipophilic fluorochrome DiOC (Fig. 2, B and C). In DiOC images (Figs. 2 though 4), the S-ER appeared, in different regions, as large tubules, as a lacework of tiny tubules, and as cisterns, all of which seemed to be interconnected components of a complex network (*12*). Mitochondria were brightly stained by DiOC (*24*) and the Ca^{2+}-sensitive dyes. Most mitochondria appeared to lie on the S-ER, which was lightly stained by DiOC and the Ca^{2+} dyes. There were, however, no mitochondria in the field imaged in Fig. 2C; most of the furaptra signal was associated with S-ER, and little signal came from organelle-free cytosolic areas (Fig. 2A).

Further Ca^{2+} images were collected during treatment with 10 μM CPA [sufficient to inhibit the S-ER Ca^{2+} pump maximally (*3*, *8*)], during subsequent addition of 10 mM CAF, and after washout of first CAF and then CPA (Fig. 2D). The CPA reversibly reduced $[Ca^{2+}]_{S\text{-}ER}$, although not uniformly, and CAF caused a further, reversible decline. Detailed changes were, however, difficult to discern from these Ca^{2+} images. To determine where $[Ca^{2+}]_{S\text{-}ER}$ declined, and by how much (*20*), we displayed data from line scans of a segment of S-ER as $[Ca^{2+}]_{S\text{-}ER}$ profiles (Fig. 2C). Initially, the mean $[Ca^{2+}]_{S\text{-}ER}$ was 110 ± 4 μM. Then, CPA caused $[Ca^{2+}]_{S\text{-}ER}$ to fall in most S-ER regions (termed CPA-sensitive) and to rise in the remainder of the S-ER (Fig. 2C). Subsequent addition of CAF caused $[Ca^{2+}]_{S\text{-}ER}$ to fall in the CAF-sensitive S-ER regions.

Many regions (≈56% of S-ER) emptied and refilled only in response to CPA addition and removal; other regions (≈22%) emptied and refilled only in response to CAF (Fig. 2C). Some S-ER regions (≈16%) (Fig. 2C) were, however, partially depleted of Ca^{2+} by CPA and were further emptied by CAF in a reversible manner. Observations with RY suggest that this overlap was associated with separate CPA-sensitive and CAF-sensitive stores that could not always be spatially resolved. A relatively larger CPA-sensitive S-ER component is consistent with observations that CPA and TG evoke larger cytosolic Ca^{2+} transients than does CAF in these cells (*4*, *8*).

When cells were twice treated with CPA, the same S-ER sites reversibly lost (or gained) Ca^{2+} during both exposures, and the same was true of cells treated with CAF (*4*). This indicates that these two types of S-ER Ca^{2+} stores are spatially distinct and specific and, thus, compartmentalized. This is consistent with known differences in the relative distribution of IP_3 and RY receptors in different types of cells (*5*, *25*), as well as the different distribution of the two receptor types within single cells (*5*).

The CAF- and CPA-sensitive stores were often demarcated by steep changes in $[Ca^{2+}]_{S\text{-}ER}$ at their boundaries (Fig. 2C). This, too, indicates that the stores are compartmentalized. Furthermore, the CAF-sensitive store must have refilled with Ca^{2+} from the cytosol during washout of CAF because $[Ca^{2+}]_{S\text{-}ER}$ did not decline in the CPA-sensitive store. This replenishment implies that Ca^{2+} was transferred between stores through the cytosol and not through the lumen of the S-ER.

Similar results were obtained with mouse (*26*) and rat astrocytes (Fig. 3A). Moreover, the CAF-releasable S-ER store also responded to RY: Regions of S-ER that filled with Ca^{2+} during exposure to CPA unloaded Ca^{2+} when RY was applied (Fig. 2E). When CPA and RY were washed out, only the CPA-sensitive regions refilled because the effects of RY were not reversible. Regions depleted of Ca^{2+} by both CPA and RY only refilled by an amount equivalent to the

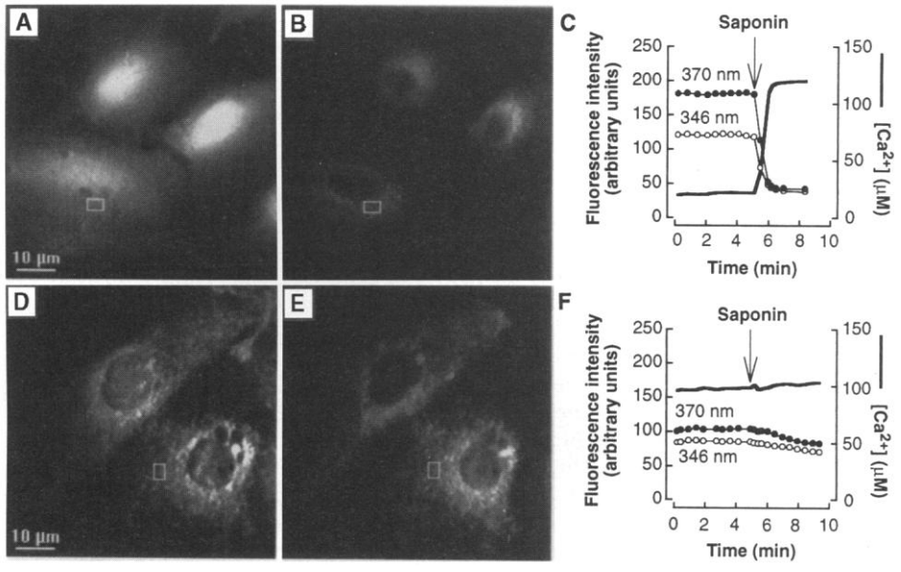

Fig. 1. Fluorescent images of furaptra-loaded primary cultured mouse cortical astrocytes. (**A** through **C**) Astrocytes loaded with furaptra at 22°C (*14*). Images (346-nm excitation, 510-nm emission) were captured before (A) and after (B) 2-min treatment with a solution of 30 μg of saponin per milliliter of Ca^{2+}-free medium. (C) Time course of (thin lines) changes in spatially averaged (within small, white rectangles in A and B) 510-nm fluorescence excited by 346- and 370-nm light (F_{346} and F_{370}) and (bold line) changes in $[Ca^{2+}]$ (*20*). Saponin was added at arrow. (**D** through **F**) Comparable data for astrocytes loaded with furaptra at 36°C (*14*). Images were captured before (D) and after (E) saponin treatment. (F) Time course of changes in fluorescence and $[Ca^{2+}]$ in the saponin-resistant intracellular stores.

CPA-induced reduction in $[Ca^{2+}]_{S\text{-}ER}$ (Fig. 2E), suggesting that the apparent overlap was associated with two different types of stores that were not spatially resolved in these regions.

We determined the time course of changes in $[Ca^{2+}]_{S\text{-}ER}$ in response to CPA and CAF in a furaptra-loaded astrocyte (Fig. 3A). The evoked changes in $[Ca^{2+}]_{S\text{-}ER}$

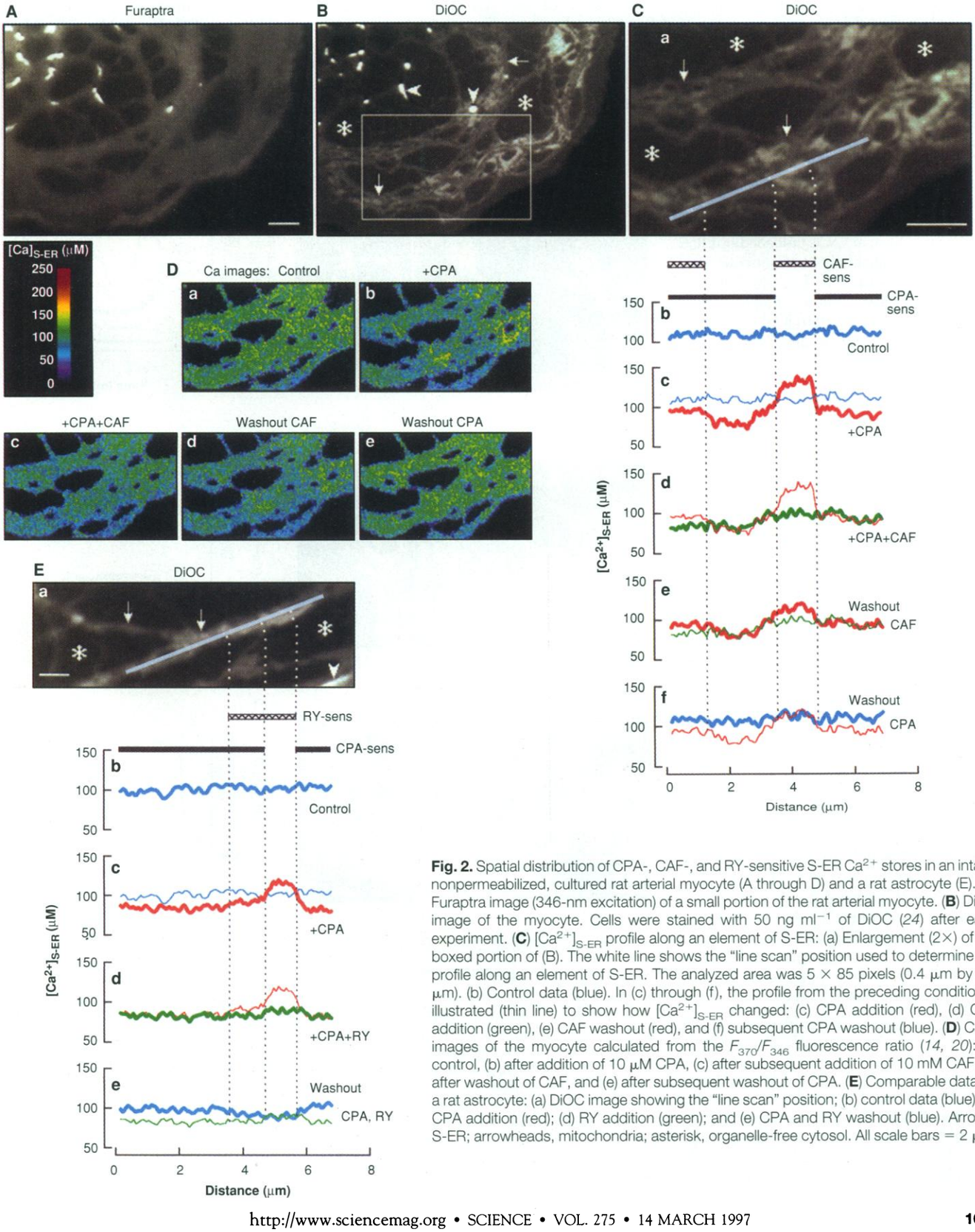

Fig. 2. Spatial distribution of CPA-, CAF-, and RY-sensitive S-ER Ca^{2+} stores in an intact, nonpermeabilized, cultured rat arterial myocyte (A through D) and a rat astrocyte (E). (**A**) Furaptra image (346-nm excitation) of a small portion of the rat arterial myocyte. (**B**) DiOC image of the myocyte. Cells were stained with 50 ng ml^{-1} of DiOC (*24*) after each experiment. (**C**) $[Ca^{2+}]_{S\text{-}ER}$ profile along an element of S-ER: (a) Enlargement (2×) of the boxed portion of (B). The white line shows the "line scan" position used to determine the profile along an element of S-ER. The analyzed area was 5 × 85 pixels (0.4 μm by 6.8 μm). (b) Control data (blue). In (c) through (f), the profile from the preceding condition is illustrated (thin line) to show how $[Ca^{2+}]_{S\text{-}ER}$ changed: (c) CPA addition (red), (d) CAF addition (green), (e) CAF washout (red), and (f) subsequent CPA washout (blue). (**D**) Ca^{2+} images of the myocyte calculated from the F_{370}/F_{346} fluorescence ratio (*14, 20*): (a) control, (b) after addition of 10 μM CPA, (c) after subsequent addition of 10 mM CAF, (d) after washout of CAF, and (e) after subsequent washout of CPA. (**E**) Comparable data for a rat astrocyte: (a) DiOC image showing the "line scan" position; (b) control data (blue); (c) CPA addition (red); (d) RY addition (green); and (e) CPA and RY washout (blue). Arrows, S-ER; arrowheads, mitochondria; asterisk, organelle-free cytosol. All scale bars = 2 μm.

(curves 1 and 2 in d correspond to CPA-sensitive and CAF- and RY-sensitive S-ER Ca^{2+} stores) were stable both spatially and temporally. Spatially averaged changes in $[Ca^{2+}]_{S\text{-}ER}$ (curve 3) were measured in the entire S-ER within the portion of the cell depicted in Fig. 3A. The distinct CPA- and CAF-sensitive compartments and the CPA-induced loading of the CAF-sensitive compartment were obscured by this spatial averaging.

Furaptra fluorescence data were presented as a 346 nm/370 nm wavelength ratio (*14*) image (Fig. 3A) rather than a Ca^{2+} image because the analyzed portion of this cell includes several mitochondria. The Ca^{2+} concentration in mitochondria ($[Ca^{2+}]_M$) rose when S-ER Ca^{2+} was unloaded by CPA and CAF, presumably because mitochondria help buffer rises in $[Ca^{2+}]_{cyt}$. The high mitochondrial 346/370 ratios might suggest that $[Ca^{2+}]_M$ is greater than $[Ca^{2+}]_{S\text{-}ER}$ even in resting cells. Other studies, however, indicate that $[Ca^{2+}]_M$ is usually much lower than $[Ca^{2+}]_{S\text{-}ER}$ (*27*). Thus, high concentrations of Mg^{2+} in mitochondria (*28*) may account for most of the mitochondrial furaptra signal. We resolved this ambiguity with the help of Ca^{2+}-selective dyes with relatively low (fura-2FF) and high (fura-2) affinities for Ca^{2+}.

The fura-2FF 360/380 ratio (*14*) was much lower in mitochondria than in the S-ER of quiescent astrocytes (Fig. 3B), implying that much of the mitochondrial furaptra signal in unstimulated cells (Fig. 3A) was due to Mg^{2+}, rather than Ca^{2+}. Most of the S-ER furaptra signal was, however, due to Ca^{2+}, because comparable values for resting $[Ca^{2+}]_{S\text{-}ER}$ in astrocytes (and in MA cells) (*26*) were obtained with fura-2FF [96 ± 3 μM, n = 8 cells (Fig. 3B)], which is insensitive to Mg^{2+}, and with furaptra [104 ± 4 μM, n = 23 cells (Figs. 2 and 3A)]. Moreover, at $[Ca^{2+}]$ >50 μM, even the furaptra signal was minimally influenced by Mg^{2+} (*17*, *22*).

Reductions and increases in $[Ca^{2+}]_{S\text{-}ER}$ evoked by CPA in spatially separate stores were also detected with fura-2FF (Fig. 3B). Resting $[Ca^{2+}]_M$ was difficult to measure accurately with fura-2FF because of the dye's low affinity for Ca^{2+}, but the large CPA-induced increases in $[Ca^{2+}]_M$ (to 7.3 ± 0.2 μM; n = 54 mitochondria from four cells) were readily detectable. Unfortunately, CAF altered fura-2FF fluorescence at the Ca^{2+}-insensitive wavelength (360 nm).

To verify that $[Ca^{2+}]_M$ was low in quiescent cells, we also measured it in astrocytes loaded at 36°C with the high-affinity (K_d = 232 nM) Ca^{2+}-selective dye fura-2 (Fig. 3C). The mean $[Ca^{2+}]_M$ (*20*) in these cells was only 195 ± 13 nM (n = 88 mitochondria from three astrocytes; MA cells yielded similar results). The addition of CPA also increased $[Ca^{2+}]_M$ in these cells (Fig. 3C), but the maximal concentration was underestimated because fura-2 is saturated by 2 to 3 μM Ca^{2+}. Because CPA also increases $[Ca^{2+}]_{cyt}$ (*8*), the cells were then treated with the mitochondrial uncoupler carbonyl cyanide *p*-trifluoromethoxyphenylhydrazone (FCCP) and the adenosine triphosphatase inhibitor oligomycin (in Ca^{2+}-free media, to minimize capacitative Ca^{2+} entry). These agents increase $[Ca^{2+}]_{cyt}$ (*29*) but reduce $[Ca^{2+}]_M$ (*30*) (Fig. 3C), confirming that $[Ca^{2+}]_M$ was measured, as opposed to $[Ca^{2+}]_{cyt}$. Thus, there are at least three functionally and spatially distinct dynamic stores of Ca^{2+} in these cells: two S-ER stores and a mitochondrial store. Mitochondria can apparently buffer cytosolic Ca^{2+} and thereby attenuate the CPA-evoked rise in $[Ca^{2+}]_{cyt}$ (*8*).

Distinction between the two types of S-ER stores did not depend on pharmaco-

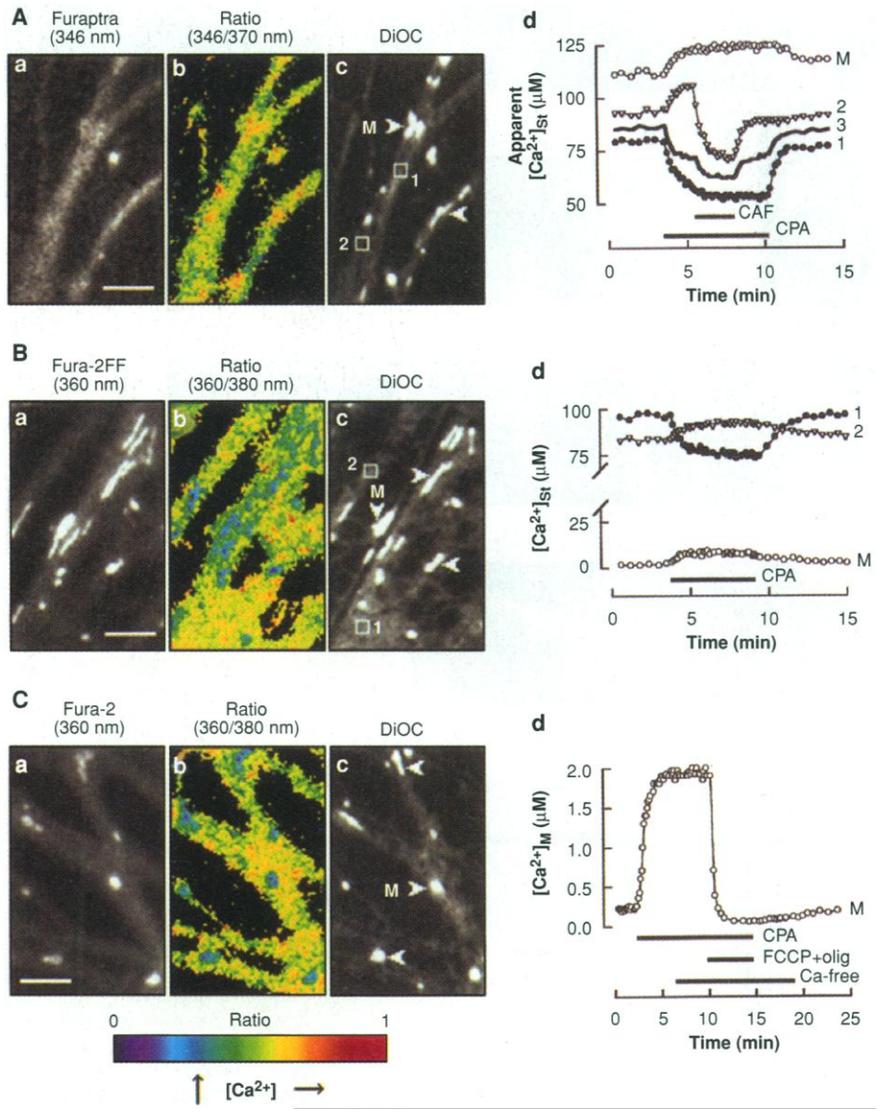

Fig. 3. Dynamic changes in $[Ca^{2+}]_M$ and $[Ca^{2+}]_{S\text{-}ER}$ in intact, nonpermeabilized rat astrocytes determined with (**A**) furaptra, (**B**) fura-2FF, and (**C**) fura-2. For all three fluorochromes: (a) dye image at the Ca^{2+}-insensitive wavelength (346 or 360 nm); (b) ratio image (346/370 nm excitation for furaptra; 360/380 nm for fura-2FF and fura-2) (*14*); (c) DiOC image; and (d) time course of changes in $[Ca^{2+}]_M$ and $[Ca^{2+}]_{S\text{-}ER}$ ($[Ca^{2+}]_{St}$ in (A) and (B) refers to both organelles; "apparent $[Ca^{2+}]_{St}$" in (A) also includes the signal from Mg^{2+}). Curves labeled M in the graphs correspond to mitochondria labeled M in the DiOC images. Curves 1 and 2 in panel d of (A) and (B) correspond to the S-ER areas within the respective small, numbered boxes in panel c; curve 3 in panel d of (A) shows the averaged $[Ca^{2+}]_{S\text{-}ER}$ for the entire S-ER area (excluding mitochondria) within panel c. "Ratio images" are shown rather than Ca^{2+} images because Ca^{2+} calibration parameters for mitochondria and S-ER were different. Arrowheads point to mitochondria; all scale bars = 2 μm.

logical methods. Compartmentalization of S-ER Ca^{2+} stores was also revealed during activation by physiological agonists. Serotonin caused $[Ca^{2+}]_{S\text{-}ER}$ to decline in most of the S-ER of a furaptra-loaded MA myocyte (Fig. 4A). In other S-ER regions, however, $[Ca^{2+}]_{S\text{-}ER}$ increased reversibly in response to serotonin. Addition of TG markedly diminished serotonin-evoked arterial contractions, but not those evoked by CAF (*31*). Indeed, CPA reversibly reduced $[Ca^{2+}]_{S\text{-}ER}$ and increased $[Ca^{2+}]_{S\text{-}ER}$ in, respectively, the same regions that were reduced and increased by serotonin (Fig. 4A). Conversely, CAF reduced $[Ca^{2+}]_{S\text{-}ER}$ in those regions in which the concentrations were increased by serotonin, and even increased $[Ca^{2+}]_{S\text{-}ER}$ in some regions that had been depleted by serotonin (Fig. 4B). The latter observation can be explained by the fact that CAF inhibits IP_3-sensitive channels (*32*) and thereby permits the IP_3-sensitive store to refill. Thus, the larger (serotonin-depletable) S-ER component (Fig. 4)

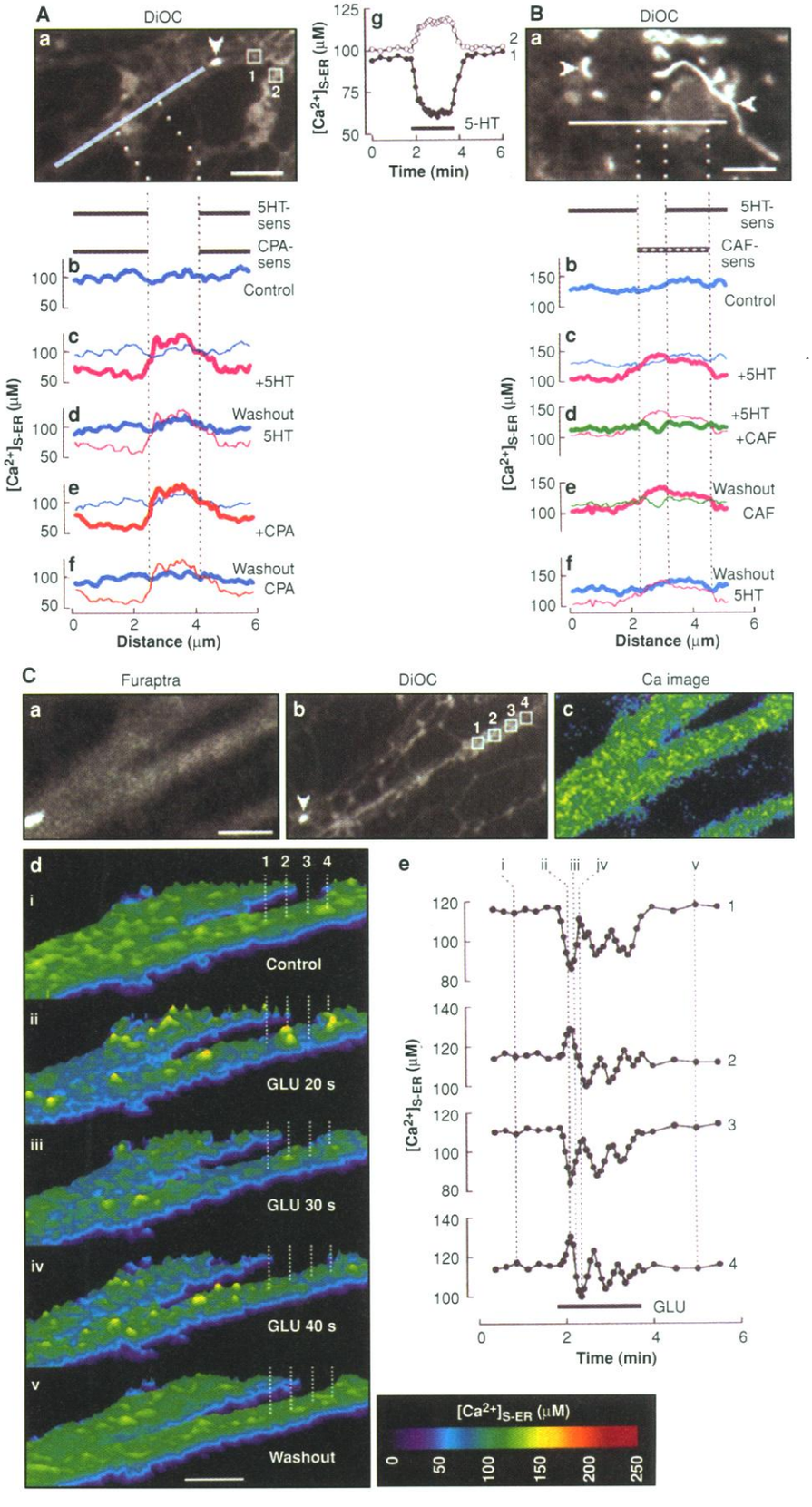

Fig. 4. Effects of physiological agonists on Ca^{2+} stores in intact, non-permeabilized cells. (**A**) Effects of serotonin (5HT) and CPA on an MA myocyte. (a) DiOC image of a portion of the cell. Long white line as in panel a of Fig. 2C. Analyzed area was 5 × 72 pixels (0.4 μm × 5.8 μm). (b) Control data. (c through f as in Fig. 2C): (c) serotonin addition (magenta), (d) serotonin washout (blue), (e) CPA addition (red), and (f) subsequent CPA washout (blue). Bars above graphs indicate S-ER regions depleted by serotonin and CPA. Serotonin and CPA depleted the same regions. (g) Time course curves that illustrate the serotonin-evoked changes in $[Ca^{2+}]_{S\text{-}ER}$ within boxes 1 and 2 in image a. (**B**) Effects of serotonin (5HT) and CAF on an MA myocyte. (a) DiOC image as in (A). Analyzed area was 5 × 64 pixels (0.4 μm × 5.1 μm). (b) Control data. (c through f as in Fig. 2C): (c) serotonin addition (magenta), (d) CAF addition (green), (e) CAF washout (magenta), and (f) subsequent serotonin washout (blue). Bars above graphs indicate S-ER regions depleted by serotonin and CAF. The CAF-sensitive regions are those in which serotonin (b through f) and CPA (Figs. 2 and 3A) raised $[Ca^{2+}]_{S\text{-}ER}$. $[Ca^{2+}]_{S\text{-}ER}$ decreased by >6 μM in 62% of the S-ER pixels, and increased by >6 μM in 32% of the S-ER pixels during serotonin exposure. The 6 μM threshold was chosen because the mean variation in $[Ca^{2+}]_{S\text{-}ER}$ in individual pixels from image to image in unstimulated cells was 5 to 7 μM. (**C**) Effects of glutamate (GLU) on a rat astrocyte. (a) Furaptra image (F_{346}) of a small portion of the cell. (b) DiOC image. Boxes 1 through 4 show the areas of S-ER analyzed in panel e. (c) Control Ca^{2+} image. (d) Contour images of $[Ca^{2+}]_{S\text{-}ER}$ distribution in this cell: (i) control; (ii through iv) $[Ca^{2+}]_{S\text{-}ER}$ distribution after 20, 30, and 40 s, respectively, of treatment with 100 μM glutamate; and (v) after washout of glutamate. (e) Time course of changes in $[Ca^{2+}]_{S\text{-}ER}$ within boxes 1 through 4 of image b; dotted vertical lines (i through v) indicate times at which $[Ca^{2+}]_{S\text{-}ER}$ distribution maps (i through v) in panel d were obtained. Arrowheads point to mitochondria; all scale bars = 2 μm.

apparently corresponds to the CPA- and TG-sensitive (and IP_3-releasable) store; the smaller component, which filled during serotonin application, is the CAF- and RY-sensitive store.

Comparable heterogeneity of S-ER responses was observed in astrocytes activated with the neurotransmitter glutamate. The responses were, however, more complex because of oscillations in $[Ca^{2+}]_{S\text{-}ER}$ (Fig. 4C) that likely underlie glutamate-evoked oscillations in $[Ca^{2+}]_{cyt}$ (*33*). Again, bath application of an agonist initially caused $[Ca^{2+}]_{S\text{-}ER}$ to decline in some parts of the S-ER but to increase in other, adjacent areas; about 20 s later, however, $[Ca^{2+}]_{S\text{-}ER}$ increased in some of the former areas and decreased in the latter. When glutamate was washed out, $[Ca^{2+}]_{S\text{-}ER}$ returned to the control level. Some detailed spatial information was obscured by the spatial averaging used for quantitative analysis of $[Ca^{2+}]_{S\text{-}ER}$ within even small ($\approx 1\ \mu m^2$) sample areas because they encompass portions of two or more compartments.

Glutamate-induced oscillations in $[Ca^{2+}]_{S\text{-}ER}$ (≈ 2 to 3 min^{-1}) were observed in most regions of the S-ER (Fig. 4C). They cannot be attributed to noise because (i) $[Ca^{2+}]_{S\text{-}ER}$ was quite steady under control conditions and after washout of glutamate (Fig. 4C) and (ii) oscillations were not observed in astrocytes treated with CPA and CAF (Figs. 2 and 3) or in arterial myocytes (Figs. 2 and 4, A and B). Moreover, the oscillation frequency was similar to that of the oscillations of $[Ca^{2+}]_{cyt}$ measured with fura-2 under comparable conditions (*26*, *33*).

Our data provide morphological evidence that the S-ER consists of two types of small, functionally discrete stores of Ca^{2+} (*34*). The physiological activity of most cells is governed by multiple Ca^{2+}-dependent mechanisms. Our results suggest that these processes may be locally controlled by spatially and temporally specific transient cytosolic Ca^{2+} signals that arise from Ca^{2+} mobilized independently from distinct, small S-ER compartments.

REFERENCES AND NOTES

1. M. J. Berridge, *Nature* **361**, 315 (1993); *ibid.* **365**, 388 (1993); R. D. Burgoyne and T. R. Cheek, *Trends. Biochem. Sci.* **16**, 319 (1991); I. M. Robinson and R. D. Burgoyne, *J. Neurochem.* **56**, 1587 (1991); T. Yamazawa, M. Iino, M. Endo, *FEBS Lett.* **301**, 181 (1992); G. Hajnoczky, C. Lin, A. P. Thomas, *J. Biol. Chem.* **269**, 10280 (1994); T. Pozzan, R. Rizzuto, P. Volpe, J. Meldolesi, *Physiol. Rev.* **74**, 595 (1994); D. E. Clapham, *Cell* **80**, 259 (1995); P. B. Simpson, R. A. J. Challiss, S. R. Nahorski, *Trends Neurosci.* **18**, 299 (1995).
2. J. Bian, T. K. Ghosh, J.-C. Wang, D. L. Gill, *J. Biol. Chem.* **266**, 8801 (1991).
3. Y. Tanaka and A. H. Tashjian Jr., *Biochemistry* **32**, 12062 (1993).
4. R. M. Tribe, M. L. Borin, M. P. Blaustein, *Proc. Natl. Acad. Sci U.S.A.* **91**, 5908 (1994).
5. P. D. Walton *et al.*, *J. Cell Biol.* **113**, 1145 (1991); K. J. Seymour-Laurent and M. E. Barish, *J. Neurosci.* **15**, 2592 (1995); S. L. Carl *et al.*, *J. Cell Biol.* **129**, 673 (1995).
6. F. S. Menniti *et al.*, *J. Biol. Chem.* **266**, 13646 (1991); Y. Sagara and G. Inesi, *ibid.*, p. 13503.
7. G. Inesi and Y. Sagara, *J. Membr. Biol.* **141**, 1 (1994).
8. V. Golovina, L. Bambrick, P. Yarowski, B. K. Krueger, M. P. Blaustein, *Glia* **16**, 296 (1996).
9. I. Bezprozvanny, J. Watras, B. E. Ehrlich, *Nature* **351**, 751 (1991).
10. M. Endo, *Physiol. Rev.* **57**, 71 (1977); E. Rousseau and G. Meissner, *Am. J. Physiol.* **256**, H328 (1989); V. Henzi and A. B. MacDermott, *Neuroscience* **46**, 251 (1992).
11. G. Meissner, *J. Biol. Chem.* **261**, 6300 (1986); F. A. Lattanzio Jr., R. G. Schlatterer, M. Nicar, K. P. Campbell, J. L. Sutko, *ibid.* **262**, 2711 (1987); P. S. McPherson and K. P. Campbell, *ibid.* **268**, 13765 (1993); R. Coronado, J. Morrissette, M. Sukhareva, D. M. Vaughan, *Am. J. Physiol.* **266**, C1485 (1994).
12. M. Terasaki, N. T. Slater, A. Fein, A. Schmider, T. S. Reese, *Proc. Natl. Acad. Sci. U.S.A.* **91**, 7510 (1994).
13. Primary cultured mouse cortical astrocytes were prepared from the brains of 17- to 18-day-old embryos (*8*); rat cortical astrocytes were prepared from 1-day-old pups (*18*). Primary cultured MA myocytes were prepared from 150-g rats (*19*). All cells were grown on 25-mm glass cover slips. Arterial myocytes lose myosin and thus cannot contract after a few days in culture [J. Chamley-Campbell, G. R. Campbell, R. Ross, *Physiol. Rev.* **59**, 1 (1979)].
14. Cells on cover slips were loaded with furaptra (*22*) by incubation (40 min at 22° or 90 min at 36°C, 5% CO_2–95% O_2) in Dulbecco's modified Eagle's culture medium containing fetal calf serum (10%) and 4 μM furaptra-AM (membrane-permeable acetoxymethyl ester of furaptra; Molecular Probes, Eugene, OR). Incubation at 36°C improved dye loading into the organelles and enabled us to study Ca^{2+} movements into and out of specific intracellular stores (*21*). Similar methods were used for loading 4 μM fura-2FF-AM (*15*) (TEFLABS, Austin, TX) and 3.3 μM fura-2-AM (Molecular Probes). Cover slips were mounted in a tissue chamber on a Nikon Diaphot microscope stage; cells were superfused with physiological salt solution (PSS) (30 min, 32° to 34°C) to remove extracellular dye and permit cellular esterases to hydrolyze the furaptra-AM. The PSS contained 140 mM NaCl, 5.9 mM KCl, 1.2 mM NaH_2PO_4, 5 mM $NaHCO_3$, 1.4 mM $MgCl_2$, 1.8 mM $CaCl_2$, 11.5 mM glucose, and 10 mM *N*-2-hydroxyethylpiperazine-*N*′-2-ethane sulfonic acid (Hepes, titrated to pH 7.4 with NaOH). We omitted $CaCl_2$ from the Ca^{2+}-free medium and added 0.05 mM EGTA. Furaptra fluorescence (370- and 346-nm excitation, 510-nm emission) was imaged as described for fura-2 (*18*); 346 nm is the Ca^{2+}-insensitive wavelength. The excitation wavelengths used for fura-2 and fura-2FF were 360 nm (Ca^{2+}-insensitive) and 380 nm. To improve the signal-to-noise ratio, we averaged 32 consecutive video frames to obtain each image.
15. R. E. London, L. A. Levy, E. Murphy, U.S. Patent 5,516,911 (1996). Fura-2FF is 2-[2(5-carboxyethyloxazole)]-5-[2-(2-bis(carboxymethylmethyl)amino-5,6-difluorophenoxy)]ethoxy-6-bis(carboxymethylmethyl)aminobenzofuran.
16. A. M. Hofer and T. E. Machen, *Proc. Natl. Acad. Sci. U.S.A.* **90**, 2598 (1993).
17. T. Sugiyama and W. F. Goldman, *Am. J. Physiol.* **269**, C698 (1995).
18. W. F. Goldman, P. J. Yarowsky, M. Juhaszova, B. K. Krueger, M. P. Blaustein, *J. Neurosci.* **14**, 5834 (1994).
19. M. K. Slodzinski, M. Juhaszova, M. P. Blaustein, *Am. J. Physiol.* **269**, C1340 (1995).
20. Intra-S-ER furaptra was calibrated in situ (*17*), with a Ca^{2+} K_d of 54 μM (*17*, *22*). Intra-store fura-2 (K_d = 0.232 μM) and fura-2FF (K_d = 35 μM) were similarly calibrated. Calculated Ca^{2+} concentrations are subject to several potential errors. Most important, perhaps, is the binding of the dye to large constituent molecules; this binding may increase the K_d substantially [S. Hollingworth, M. Zhao, S. M. Baylor, *J. Gen. Physiol.* **108**, 455 (1996)], thereby causing us to underestimate $[Ca^{2+}]$, which is directly proportional to K_d [G. Grynkiewicz, M. Poenie, R. Y. Tsien, *J. Biol. Chem.* **260**, 3440 (1985)]. Our calculated resting $[Ca^{2+}]_{S\text{-}ER}$, ≈110 μM in furaptra-loaded cells, is comparable to values obtained with mag-indo-1 in intact cells, 30 to 230 μM [F. W. Tse, A. Tse, B. Hille, *Proc. Natl. Acad. Sci. U.S.A.* **91**, 9750 (1994)] and with furaptra (mag-fura-2) in saponin-permeabilized cells (*16*, *17*), as well as with fura-2FF (≈100 μM). In contrast, values of ≈260 μM [A. M. Hofer and I. Schulz, *Cell Calcium* **20**, 235 (1996)] and ≈630 μM (*35*) were obtained with furaptra by assuming that intra-S-ER dye was saturated with Ca^{2+}, contrary to our observations (Figs. 2 through 4) and theirs [for example, figure 3 in (*35*)]. A higher $[Ca^{2+}]_{S\text{-}ER}$ (≈2 to 3 mM) was obtained with an aequorin analog targeted to the S-ER, and calibrated with Sr^{2+} [M. Montero *et al.*, *EMBO J.* **14**, 5467 (1995)]. These uncertainties do not, however, undermine our basic observations regarding S-ER compartments and changes in their Ca^{2+} content.
21. M. C. Glennon *et al.*, *J. Biol. Chem.* **267**, 25568 (1992).
22. M. Konishi, S. Hollingworth, A. B. Harkins, S. M. Baylor, *J. Gen. Physiol.* **97**, 271 (1991).
23. B. Raju, E. Murphy, L. A. Levy, R. D. Hall, R. E. London, *Am. J. Physiol.* **256**, C540 (1989); E. Murphy, *Miner. Electrolyte Metab.* **19**, 250 (1993).
24. M. Terasaki, *Methods Cell Biol.* **29**, 125 (1989).
25. V. Sorrentino and P. Volpe, *Trends Pharmacol. Sci.* **14**, 98 (1993).
26. V. Golovina and M. P. Blaustein, unpublished data.
27. M. Miyata *et al.*, *Am. J. Physiol.* **261**, H1123 (1991); S. P. Allen, V. M. Darley-Usmar, J. G. McCormack, D. Stone, *J. Mol. Cell. Cardiol.* **25**, 949 (1993); S.-S. Sheu and M.-J. Jou, *J. Bioenerg. Biomembr.* **26**, 487 (1994); A. M. Lawrie, R. Rizzuto, T. Pozzan, A. W. M. Simpson, *J. Biol. Chem.* **271**, 10753 (1996).
28. D. W. Jung, C. J. Chapman, K. Baysal, D. R. Pfeiffer, G. P. Brierley, *Arch. Biochem. Biophys.* **332**, 19 (1996).
29. X.-J. Yuan, T. Sugiyama, W. F. Goldman, L. J. Rubin, M. P. Blaustein, *Am. J. Physiol.* **270**, C321 (1996).
30. M. R. Duchen and T. J. Biscoe, *J. Physiol. (London)* **450**, 33 (1992); G. Isenberg, S. Han, A. Schiefer, M.-F. Wendt, *Cardiovasc. Res.* **27**, 1800 (1993); D. D. Friel and R. W. Tsien, *J. Neurosci.* **14**, 4007 (1994).
31. H. Shima and M. P. Blaustein, *Circ. Res.* **70**, 968 (1992).
32. I. Parker and I. Ivora, *J. Physiol. (London)* **433**, 229 (1991); G. R. Brown, L. G. Sauyers, C. J. Kirk, R. H. Michell, F. Michelangeli, *Biochem. J.* **282**, 309 (1992); I. Bezprozvanny, S. Bezprozvannaya, B. E. Ehrlich, *Mol. Biol. Cell* **5**, 97 (1994).
33. A. H. Cornell-Bell, S. M. Finkbeiner, M. S. Cooper, S. J. Smith, *Science* **247**, 470 (1990); A. M. Jensen and S. Y. Chiu, *J. Neurosci.* **10**, 1165 (1990).
34. I. Parker and Y. Yao, *Proc. R. Soc. London Ser. B* **246**, 269 (1991); T. R. Cheek *et al.*, *Biochem. J.* **301**, 879 (1994).
35. J.-Y. Chatton, H. Liu, J. W. Stucki, *FEBS Lett.* **368**, 165 (1995).

36. We thank E. M. Santiago for arterial cell cultures, G. McNamara for help with imaging software, G. R. Monteith for recommending fura-2FF, R. S. Rogowski for technical assistance, R. J. Bloch, M. L. Borin, B. K. Krueger, W. J. Lederer, G. R. Monteith, I. Parker, J. B. Wade, and W. G. Wier for comments on the manuscript, and L. Pavarotti for setting the mood for image analysis. Supported by NIH grants NS-16106 and HL-32276 and by funds from the University of Maryland at Baltimore School of Medicine and Graduate School.

14 March 1996; accepted 23 January 1997